doi:10.1038/nature10666

Our GCM is based on the Flexible Modeling System of the Geophysical Fluid Dynamics Laboratory (http://fms.gfdl.noaa.gov). It is similar to standard models for Earth's atmosphere, but with Titan's radius, planetary rotation rate, material properties, and seasonally varying insolation, and with a methane cycle instead of a water cycle. The GCM has similarities to the models in refs. 16, 17, but unlike those, it is 3D and eddy-resolving and has a different representation of radiative transfer and surface processes.

Resolution. The GCM solves the hydrostatic primitive equations in vorticity-divergence form, using the spectral transform method in the horizontal and finite differences in the vertical[31]. The horizontal spectral resolution is T21 (corresponding to about $5^\circ \times 5^\circ$ resolution of the transform grid). The vertical coordinate is $\sigma = p/p_s$ (pressure p normalized by surface pressure p_s); it is discretized with 18 unequally spaced levels[32]. The top of the model is at $\sigma = 0$; the uppermost full level has a mean pressure of 15 mbar (altitude $\sim$90 km). The time-stepping scheme is a semi-implicit leapfrog scheme (timestep 1600 s).

Methane thermodynamics. Methane is advected with a finite-volume scheme on the transform grid. A large-scale condensation scheme ensures that the mean relative humidity in a grid cell does not exceed 100% relative to saturation over a binary methane-nitrogen mixture (saturation vapor pressure 10600 Pa at 90.68 K)[33]. Condensing methane precipitates, and condensate on the grid scale re-evaporates into the air it falls through until that air is saturated. Only the vapor-liquid phase transition is considered, and the latent heat of vaporization is taken to be constant ($L = 4.9 \times 10^5\,\mathrm{J\,kg^{-1}}$), as in refs. 16, 17, 34 (that is, methane freezing is neglected). The latent heat is smaller than that for pure methane to approximately take its reduction for a binary methane-nitrogen mixture into account[33]. Thermodynamic effects of ethane on the mixture[35] are not explicitly taken into account.

Moist convection. A quasi-equilibrium convection scheme[36] represents moist convection. It is adapted for methane thermodynamics, takes the effects of methane on the air density into account[34], and relaxes convectively unstable atmospheric columns on a timescale of 4 hrs toward a moist pseudoadiabat with a relative humidity of 70%.

This is an idealized representation of moist convection. Like other quasi-equilibrium moist convection schemes, it likely underestimates precipitation rates in extreme events; however, mean precipitation rates (which are more strongly energetically constrained) are likely more adequately simulated[37].

Radiative transfer. Radiative transfer is represented using the two-stream approximation. It assumes an atmosphere with horizontally homogeneous composition and with wavelength-independent transfer of solar radiation and thermal radiation, ignoring poorly constrained pro-

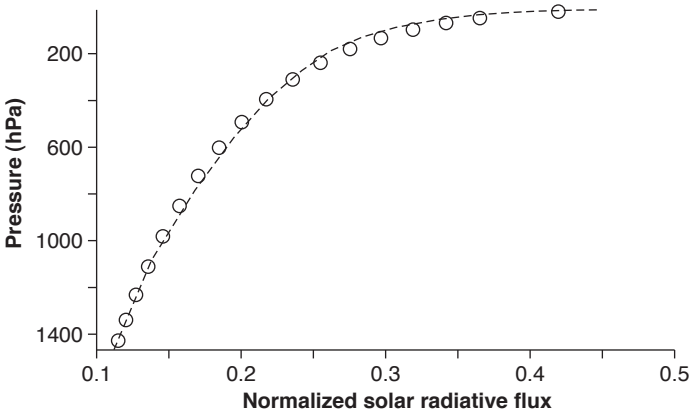

Supplementary Figure 1: Net solar radiative flux normalized by the incident flux at the top of the atmosphere in GCM and measured on Titan. Dashed line: Solar radiative flux inferred from Descent Imager/Spectral Radiometer data obtained by the Huygens probe[41]. (The flux is interpolated from altitude to pressure levels using data obtained by the Huygens Atmospheric Structure Instrument[43].) Circles: Solar radiative flux at the vertical coordinate levels in the GCM. In the GCM, the normalized solar radiative flux is spatially and temporally constant; only the incident flux at the top of the atmosphere varies with latitude and time.

cesses such as cloud-radiative feedbacks. Saturn's seasonally varying insolation is imposed at the top of atmosphere, taking into account the current orbital configuration (eccentricity, obliquity, and longitude of perihelion); we ignore diurnal insolation variations because the large thermal inertia of the atmosphere is expected to strongly damp diurnal temperature variations.

Solar radiation is scattered and absorbed in the atmosphere, assuming diffuse incidence and multiple scattering[38], with asymmetry factor 0.65 and single-scattering albedo 0.95. The solar extinction optical depth is specified as

$$\tau_s = \tau_{s0}(p/p_0)^\gamma,$$

with optical thickness $\tau_{s0} = 5$ at $p_0 = 1.467\times10^5$ Pa and empirical exponent $\gamma = 0.21$. The surface albedo is 0.3 uniformly, implying a planetary Bond albedo of 0.20 given the radiative transfer prescription and its parameters. The parameters are chosen to approximate optical properties of the surface[39] and of atmospheric aerosols[40] and to give a good fit to measured solar radiative fluxes; within our GCM domain, they imply net solar radiative fluxes that are within 6% of those measured by the Huygens probe[41] (Supplementary Fig. 1).

Thermal radiation is absorbed in the atmosphere, with an optical depth

$$\tau_l = \tau_{l0}\left[\alpha(p/p_0)^2 + (1-\alpha)(p/p_0)\right]$$

that roughly represents a mixture of collision-induced absorption (quadratic term, weight $\alpha = 0.85$) and absorption by a well-mixed absorber (linear term, weight $1-\alpha = 0.15$). The thermal optical thickness of the atmosphere is $\tau_{l0} = 10$ (cf. ref. 42).

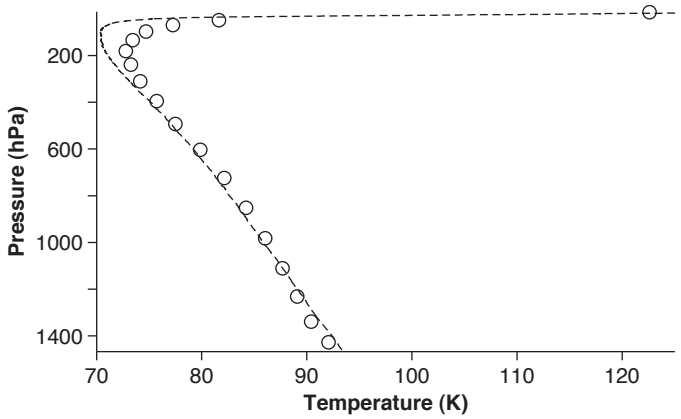

Supplementary Figure 2: Thermal structure at Huygens landing site in GCM and measured on Titan. Dashed line: Temperature measured by the Huygens Atmospheric Structure Instrument at $10.2°$S on 14-January-2005[43]. Circles: Mean temperature at the corresponding latitude and time (9.1 yrs past autumnal equinox) at the vertical coordinate levels of the GCM.

In the statistically steady state of the GCM, this formulation of radiative transfer results in a realistic temperature profile with a tropopause, without the need to invoke discrete haze layers or cloud decks; in the lower troposphere, temperatures are within l K and near the tropopause within ~ 5 K of those measured by the Huygens probe[43] (Supplementary Fig. 2).

Boundary layer. A k-profile scheme represents boundary-layer turbulence[44]. Surface fluxes of momentum, sensible heat, and methane (where available) are calculated using standard bulk aerodynamic formulae, with exchange coefficients determined from Monin-Obukhov similarity theory, a roughness length of $5 \times 10^{-3}\,\mathrm{m}$, and an additive gustiness term of $0.1\,\mathrm{m\,s^{-1}}$ in surface velocities to represent subgrid-scale wind fluctuations. (In the bulk aerodynamic formula for methane fluxes, we do not use an additional "methane availability parameter" as in some other studies[17,45].) Our results are not sensitive to the choice of these parameters.

Subgrid-scale dissipation. Horizontal ∇^8 hyperdiffusion in the vorticity, divergence, temperature, and specific humidity equations represents unresolved turbulent dissipation. The hyperdiffusion coefficient is chosen to give a damping time scale of 3 hrs at the smallest resolved scale. (Sufficient subgrid-scale dissipation is essential for the robustness of our results. Simulations with insufficient subgrid-scale dissipation of specific humidity resulted in grid-scale noise and surface methane reservoirs with large variations across narrow latitude bands, similar to what is seen in simulations in ref. 16; these were numerical artifacts.) In the uppermost model layer, horizontal diffusion damps vorticity and divergence variations (diffusivity $5 \times 10^7\,\mathrm{m^2\,s^{-1}}$).

Surface reservoir. Surface methane hydrology is represented by a simplified bucket model[46]. Where surface methane is available, the evaporation rate is given by the bulk aerodynamic formula; where none is available, the evaporation rate vanishes. The surface methane level in each grid cell

increases or decreases according to the local rates of precipitation and evaporation. Additionally, methane diffuses along the surface (diffusivity $100\,\mathrm{m^2\,s^{-1}}$), as a simple representation of relatively slow surface flows.

Surface energy balance. The surface temperature evolves according to the surface energy balance of a homogenous slab with heat capacity $2.5 \times 10^5\,\mathrm{J\,m^{-2}\,K^{-1}}$ (similar to that of a porous icy regolith[47]) , with temperature tendencies balanced by insolation, thermal radiative fluxes, and the surface fluxes of sensible heat and latent heat (methane evaporation). The value of the slab heat capacity does not substantially affect our results, as long as it is much smaller than the heat capacity of the atmosphere ($\sim 10^8\,\mathrm{J\,m^{-2}\,K^{-1}}$).

Initialization, simulations, and parameter sensitivity. We carried out simulations with various ways of initializing the atmosphere and surface methane reservoir (adding small random perturbations in the atmosphere to break the axisymmetry of the initial state). The simulation described in the main paper was initialized with a dry surface and with an isothermal (86 K) atmosphere containing the equivalent of 12 m of liquid methane distributed uniformly. The total amount of methane in the atmosphere-ocean system is (up to small numerical inaccuracies) conserved in the GCM. We obtained a statistically steady state in a long spin-up period (135 Titan years, with 1 Titan year = 10758 Earth days)—much longer than those used in previous studies[16–18,45]. The results we show are averages over 25 Titan years in the statistically steady state.

Our central results are insensitive to how the simulations are initialized, provided a statistically steady state is reached (which, depending on the initial condition, can take $\gtrsim 100$ Titan years because of the small net precipitation differences between the hemispheres). For example, a simulation initialized with a dry isothermal atmosphere and with 12 m of methane uniformly at the surface eventually produces a statistically steady state that is indistinguishable from that of the simulation described in the main paper. With less than $\sim$7 m of methane initially, the surface dries out completely, as in ref. 16; with somewhat more methane initially, the southern methane reservoir is only seasonally filled. Generally, with more methane initially, more accumulates at the poles, and the equatorward extent of the polar reservoirs increases, but the amount of methane in the atmosphere does not increase substantially beyond $\sim$7 m. The equatorward extent of the polar reservoirs also increases with the along-surface diffusivity. However, the formation of polar reservoirs is a robust result that occurs with a variety of methane amounts and diffusivities.

While our GCM reproduces the observed surface temperature distribution[30] and tropospheric vertical temperature profile (Fig. 2) relatively well, it only reproduces qualitative aspects of the zonal wind distribution. For example, it does produce equatorial superrotation, as is observed[21], but the tropospheric zonal winds are generally weaker than those observed (up to 2–3 $\mathrm{m\,s^{-1}}$ in the upper troposphere of the GCM vs. over 10 $\mathrm{m\,s^{-1}}$ inferred from the Huygens descent[21]). We will discuss the wind structure and the underlying dynamics in more detail elsewhere.

Supplementary References

31. Durran, D. R. *Numerical Methods for Wave Equations in Geophysical Fluid Dynamics*, vol. 32 of *Texts in Applied Mathematics* (Springer, New York, 1999).

32. Simmons, A. J. & Burridge, D. M. An energy and angular-momentum conserving vertical finite-difference scheme and hybrid vertical coordinates. *Mon. Wea. Rev.* **109**, 758–766 (1981).

33. Thompson, W. R., Zollweg, J. A. & Gabis, D. H. Vapor-liquid equilibrium thermodynamics of N2 + CH4: Model and Titan applications. *Icarus* **97**, 187–199 (1992).

34. O'Gorman, P. A. & Schneider, T. The hydrological cycle over a wide range of climates simulated with an idealized GCM. *J. Climate* **21**, 3815–3832 (2008).

35. Graves, S. D. B., McKay, C. P., Griffith, C. A., Ferri, F. & Fulchignoni, M. Rain and hail can reach the surface of Titan. *Planet. Space Sci.* **56**, 346–357 (2008).

36. Frierson, D. M. W. The dynamics of idealized convection schemes and their effect on the zonally averaged tropical circulation. *J. Atmos. Sci.* **64**, 1959–1976 (2007).

37. Sun, Y., Solomon, S., Dai, A. & Portmann, R. W. How often does it rain? *J. Climate* **19**, 919–934 (2006).

38. Petty, G. W. *A First Course in Atmospheric Radiation* (Sundog Publishing, Madison, Wisconsin, 2006), 2nd edn.

39. Schröder, S. E. & Keller, H. U. The reflectance spectrum of Titan's surface at the Huygens landing site determined by the descent imager/spectral radiometer. *Planet. Space Sci.* **56**, 753–769 (2008).

40. Tomasko, M. G. & West, R. A. Aerosols in Titan's atmosphere. In Brown, R. H., Lebreton, J.-P. & Waite, J. H. (eds.) *Titan from Cassini-Huygens*, chap. 12, 297–321 (Springer, 2009).

41. Tomasko, M. *et al.* Heat balance in Titan's atmosphere. *Planet. Space Sci.* **56**, 648–659 (2008).

42. McKay, C. P., Pollack, J. B. & Courtin, R. The greenhouse and antigreenhouse effects on Titan. *Science* **253**, 1118–1121 (1991).

43. Fulchignoni, M. *et al.* In situ measurements of the physical characteristics of Titan's environment. *Nature* **438**, 785–791 (2005).

44. Troen, I. B. & Mahrt, L. A simple model of the atmospheric boundary layer: Sensitivity to surface evaporation. *Boundary-Layer Met.* **37**, 129–148 (1986).

45. Tokano, T. Impact of seas/lakes on polar meteorology of Titan: Simulation by a coupled GCM-sea model. *Icarus* **204**, 619–636 (2009).

46. Manabe, S. Climate and the ocean circulation: I. The atmospheric circulation and the hydrology of the Earth's surface. *Mon. Wea. Rev.* **97**, 739–773 (1969).

47. Tokano, T. Meteorological assessment of the surface temperatures on Titan: Constraints on the surface type. *Icarus* **173**, 222–242 (2005).